

RESEARCH ARTICLE

A simplified empirical model to estimate oxygen relaxivity at different magnetic fields

Emma Bluemke  | Eleanor Stride  | Daniel Peter Bulte

Institute of Biomedical Engineering,
Department of Engineering Sciences,
University of Oxford, UK

Correspondence

Emma Bluemke, Old Road Campus Research
Building, University of Oxford, Headington,
Oxford OX3 7DQ, UK.
Email: emma.bluemke@new.ox.ac.uk

Funding information

Engineering and Physical Sciences Research
Council (EPSRC) and Medical Research Council
(MRC), Grant/Award Number: EP/L016052/1;
Clarendon Scholarship fund; EPSRC, Grant/
Award Numbers: EP/S021507/1, EP/
L024012/1

The change in longitudinal relaxation rate (R_1) produced by oxygen has been used as a means of inferring oxygenation levels in magnetic resonance imaging in numerous applications. The relationship between oxygen partial pressure (pO_2) and R_1 is linear and reproducible, and the slope represents the relaxivity of oxygen (r_{1Ox}) in that material. However, there is considerable variability in the values of r_{1Ox} reported, and they have been shown to vary by field strength and temperature. Therefore, we have compiled 28 reported empirical values of the relaxivity of oxygen as a resource for researchers. Furthermore, we provide an empirical model for estimating the relaxivity of oxygen in water, saline, plasma, and vitreous fluids, accounting for magnetic field strength and temperature. The model agrees well ($R^2 = 0.93$) with the data gathered from the literature for fields ranging from 0.011 to 8.45 T and temperatures of 21–40 °C. This provides a useful resource for researchers seeking to quantify pO_2 in simple fluids in their studies, such as water and saline phantoms, or bodily fluids such as vitreous fluids, cerebrospinal fluids, and amniotic fluids.

KEYWORDS

longitudinal relaxation, oxygen, R_1 , relaxivity, vitreous, water

1 | INTRODUCTION

Many researchers have investigated using the paramagnetic relaxivity effect of oxygen on longitudinal relaxation as a means of inferring oxygenation levels for applications ranging from cancer therapy to seawater analysis.^{1–5} For example, measurements of the longitudinal relaxation rate R_1 ($1/T_1$) have been used to infer oxygen levels in vitreous fluid as a noninvasive alternative to the highly invasive oxygen electrodes used to measure retinal hypoxia,^{6–8} bladder urine⁹ and urine in the renal pelvis to create a noninvasive detection of renal dysfunction,⁵ and cerebrospinal fluid,^{9,10} and this relationship between pO_2 and R_1 is also the basis for oxygen-enhanced MRI techniques.^{11–13} In the linear relationship between pO_2 and R_1 , the slope represents the relaxivity of oxygen, or r_{1Ox} , in that material. Unfortunately, however, there is considerable variability in the values reported for r_{1Ox} from empirical measurements, and consequently reliable quantification of pO_2 from R_1 measurements presents a challenge.

This paper provides a summary of the empirical measurements reported in the literature, investigating the relationship between R_1 and the partial pressure of oxygen in phantoms, saline and water solutions, and vitreous fluid. These experiments have been performed using different equipment and field strengths and reported with a variety of units. For consistency, therefore, all T_1 values will be reported in ms, R_1 in s^{-1} , and relaxivity in s^{-1}/mmHg oxygen, with the corresponding field strength, temperature and material specified where these data are available. We then

Abbreviations: AIC, Akaike information criterion; B_0 , main static magnetic field in MRI scanner; MSE, mean squared error; pO_2 , partial pressure of oxygen; R_1 , longitudinal relaxation rate; r_{1Ox} , relaxivity of oxygen.

This is an open access article under the terms of the Creative Commons Attribution License, which permits use, distribution and reproduction in any medium, provided the original work is properly cited.

© 2021 The Authors. *NMR in Biomedicine* published by John Wiley & Sons Ltd.

propose a simplified empirical model for estimating r_{1Ox} in water, saline, plasma, and vitreous fluids based on these reported literature values and report the resulting model parameters. Our aim is to provide a useful review and tool for researchers seeking to quantify pO_2 in simple fluids, such as water and saline phantoms, or bodily fluids such as vitreous fluids, cerebrospinal fluids, and amniotic fluids. This model does not represent the r_{1Ox} in blood or tissue, due to the addition of proteins, structure, cells, lipids, and deoxyhemoglobin, which will affect the R_1 - pO_2 relationship, to be addressed in a separate manuscript.

2 | METHODS

2.1 | Model theory

T_1 (measured in ms), and its inverse, R_1 (typically reported in s^{-1}), have both been used in the literature when reporting the relaxivity effect of oxygen. R_1 is linearly dependent on the concentration of paramagnetic particles,^{14,15} in this case dissolved molecular oxygen in the solution, with the following equation:

$$R_{1Ox} = R_{1,0} + r_{1Ox}C \quad (1)$$

where R_{1Ox} is the relaxation rate in the solution with oxygen added, $R_{1,0}$ is the relaxation rate in the solution without oxygen, C is the concentration or partial pressure of oxygen, and r_{1Ox} is the relaxivity of oxygen in that solution (whose units depend on the oxygen measurement used in the constant C) (shown in Figure 1). Since the partial pressure of oxygen (pO_2) is a common measurement in biomedicine and clinical applications, in this manuscript, we report C as pO_2 in mmHg and r_{1Ox} in s^{-1}/mmHg . Conversion factors to other common units such as kPa, Torr, mmol/L, mg/L, and mL/L can be found in Supplementary Table S1.

Changes in both T_1 and R_1 have been used to report changes in pO_2 in the past.¹⁶ However, although an increase in oxygen could still qualitatively roughly be inferred from a shortening of T_1 , it is important to note that the linear relationship exists with $1/T_1$ (R_1)—not T_1 —and

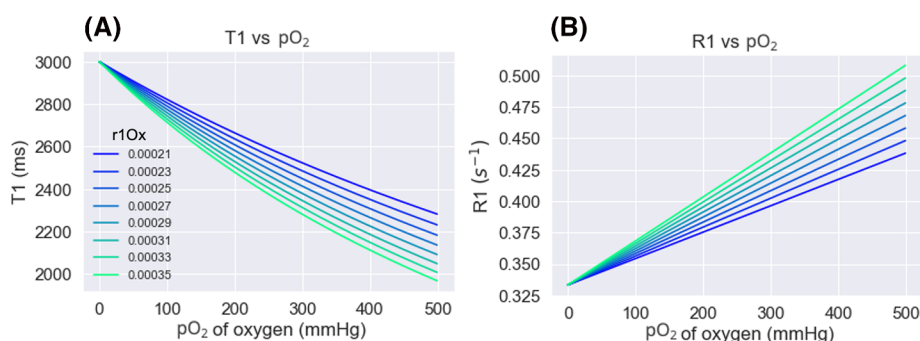


FIGURE 1 The relationship between T_1 and pO_2 (A) and R_1 and pO_2 (B) in a solution, with the initial T_1 of 3000 ms. The values are calculated using a range of r_{1Ox} (relaxivity) reported in the literature at 1.5 T, in units s^{-1}/mmHg oxygen

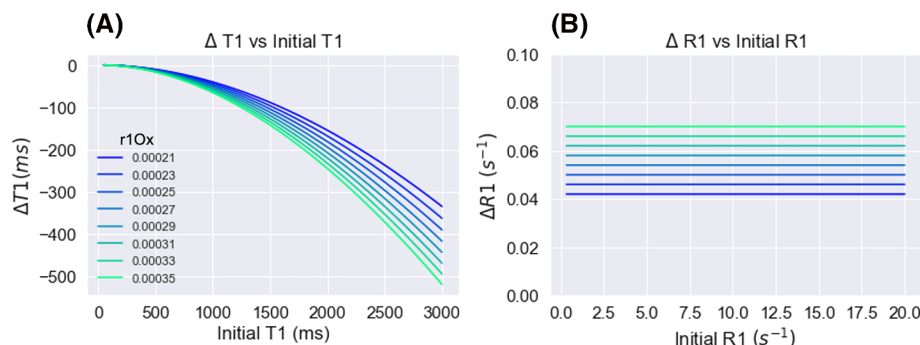


FIGURE 2 The relationship between ΔT_1 and initial T_1 (A) and ΔR_1 and initial R_1 (B), for a ΔpO_2 of 200 mmHg. The values are calculated using a range of r_{1Ox} (relaxivity) reported in the literature at 1.5 T, in units s^{-1}/mmHg oxygen

therefore the change in T_1 caused by oxygen will be dependent on the original T_1 (shown in Figure 2). Therefore, for a quantitative inference of pO_2 change it is necessary to discuss changes with respect to R_1 .

The r_{1Ox} , or relaxivity of oxygen, is affected by various experimental factors, including field strength. Equations already exist to determine the relationship between field strength and R_1 ; in 2001, Teng et al.¹⁷ measured the proton spin-lattice relaxation rate in water as a function of magnetic field strength at 1 atm of oxygen (approximately 760 mmHg) and found that the magnetic relaxation dispersion due to the paramagnetic contribution from molecular oxygen is well approximated by a Lorentzian shape, for which they proposed the following equation:

$$\frac{1}{T_{1Ox}} = A \frac{\tau}{1 + \tau^2 \omega_s^2} + B \quad (2)$$

where A and B are constants, ω_s is the electron Larmor frequency, and τ is the correlation time for the electron-nuclear coupling (empirically measured to be 6.8 ± 0.5 ps in water).¹⁷ One variable of particular interest for medical imaging research is field strength, which can be related to the electron Larmor frequency above (ω_s) by the electron gyromagnetic ratio ($\gamma_e = 1.76 \times 10^{11}$ rad s⁻¹ T⁻¹) and Larmor equation $\omega_s = \gamma_e B_0$. By substituting $\omega_s = \gamma_e B_0$ into Equation 2, we can see that

$$\frac{1}{T_{1Ox}} = A \frac{\tau}{1 + \tau^2 \gamma_e^2 B_0^2} + B. \quad (3)$$

From Equation 1 we know that $1/T_{1Ox}$ is proportional to the relaxivity (r_{1Ox}), and from Reference 17 we know that the Lorentzian magnetic relaxation dispersion is due to the paramagnetic contribution from molecular oxygen. Therefore, we propose that the relationship between r_{1Ox} and field strength will be well approximated by a similar Lorentzian equation with new constants:

$$r_{1Ox} = \frac{C_1}{1 + C_2 B_0^2} + C_3 \quad (4)$$

where C_1 , C_2 , and C_3 are new constants, and B_0 is the magnetic field strength (T). It is worth noting that in Equation 4 C_1 will not be equal to $A\tau$ as it is in Equation 3, since Equation 3 is calculating R_1 and Equation 4 is calculating r_{1Ox} —while R_1 and r_{1Ox} should be proportional, there are additional multiplying or dividing factors that will be encompassed by C_1 .

Finally, the relaxivity of oxygen is also reported to be affected by temperature, as seen in the varied relaxivity measurements reported by Muir et al.⁸ To account for this, we add a fourth constant (C_{Temp}), which represents the linear slope of relaxivity change due to temperature, resulting in the final equation:

$$r_{1Ox} = \frac{C_1}{1 + C_2 B_0^2} + C_3 + C_{Temp} * T. \quad (5)$$

2.2 | Data collection and analysis

The 28 reported values for oxygen relaxivity were collected from the literature, and all units were converted to s⁻¹/mmHg oxygen, shown in Table 1 alongside the field strength and material used in each experiment. If data extraction from graphs was necessary, a digital plot analyzer was used to reliably extract values.²⁵

The SciPy *optimize* function for nonlinear least-squares fitting was used.²⁶ Equation 5 was fitted using a randomized subset of 90% of the 28 literature data points in Table 1, fitting the B_0 and temperature values simultaneously. The dataset was split into randomized subsets for fitting using the sklearn *train_test_fit* function with shuffling.²⁷ This process was iterated 1000 times, and the median and 95% confidence interval of the distribution of fitted values for each parameter were used as the final parameters (listed in Table 2). Violin plots showing the distribution of parameter estimates from each iteration are shown in Supplementary Figure S1. Following the model fitting, all four final parameter values were substituted into Equation 5, and the accuracy of the model's predicted r_{1Ox} was compared against the 'true' r_{1Ox} values, shown in Figure 3.



TABLE 1 A collection of 28 reported values for oxygen relaxivity from the literature with all units as s^{-1}/mmHg oxygen alongside the field strength and material used in each experiment. Temperature is indicated where it was reported. The MRI acquisition details from each experiment are listed in Supplementary Table S4

Reference	r_{1Ox} (s^{-1}/mmHg) $\times 10^{-4}$	Field strength (T)	Temp. ($^{\circ}\text{C}$)	Material
Matsumoto et al., 2006 ¹⁸	2.17	4.7	37	Saline
Zaharchuk et al., 2005 ¹⁰	2.7	1.5	37	Saline
d'Othée et al., 2003 ¹⁶	1.38	8.45	21	Saline
d'Othée et al., 2003 ¹⁶	1.90	1.5	21	Saline
Kramer et al., 2013 ¹⁹	2.82	1.5	37*	Saline
Kramer et al., 2013 ¹⁹	2.21	3	37*	Saline
Simpson et al., 2013 ⁷	3.6	1.5	35	Saline
Pilkinton et al., 2012 ²⁰	1.61	3	37	Water
Vatnehol et al., 2020 ²¹	1.9	3	22	Water
Nestle et al., 2003 ³	4.2	0.5	22	Water
Hausser and Noack, 1965 ²²	3.72	0.63	22	Water
Zaharchuk et al., 2006 ⁹	2.49	1.5	37	Water
Graf et al., 1980 ²³	6.60	0.011	25	Water
Graf et al., 1980 ²³	6.60	0.031	25	Water
Graf et al., 1980 ²³	6.23	0.051	25	Water
Graf et al., 1980 ²³	6.60	0.137	25	Water
Graf et al., 1980 ²³	6.13	0.259	25	Water
Graf et al., 1980 ²³	5.18	0.525	25	Water
Graf et al., 1980 ²³	3.68	0.713	25	Water
Graf et al., 1980 ²³	3.89	0.159	25	Water
Graf et al., 1980 ²³	2.74	2.139	25	Water
Graf et al., 1980 ²³	2.51	4.387	25	Water
Muir et al., 2013 ⁸	2.04	3	34	Water
Muir et al., 2013 ⁸	2.05	3	37	Water
Muir et al., 2013 ⁸	2.11	3	40	Water
Simpson et al., 2013 ⁷	3.47	1.5	35	Vitreous fluid
d'Othée et al., 2003 ¹⁶	1.11	8.45	21	Plasma (ex vivo)
Hueckel et al., 2000 ²⁴	3.38	1.5	37	Plasma (ex vivo)

*Temperature not reported, assumed to be 37 $^{\circ}\text{C}$.

TABLE 2 A summary of the final FOUR parameter estimates from the model fitting. Multiply the final model r_{1Ox} result by 10^4 to obtain a relaxivity in units of s^{-1}/mmHg

Parameter name	Resulting value from fit (95% lower and upper confidence intervals)	Units*
C_1	4.87 (4.70, 5.04)	$10^{-4} s^{-1}/\text{mmHg}$
C_2	1.99 (1.59, 2.38)	T^{-2}
C_3	0.844 (0.452, 1.24)	$10^{-4} s^{-1}/\text{mmHg}$
C_{Temp}	0.0323 (0.0211, 0.0434)	$10^{-4} s^{-1}/\text{mmHg}/^{\circ}\text{C}^*$

*If using temperature in Kelvin, subtract 273.15 to convert your temperature to $^{\circ}\text{C}$.

3 | RESULTS

As shown in Table 1, we found 28 total measurements of r_{1Ox} : 7 measured in saline solutions,^{7,9,16,18,19} 18 in water,^{3,8,9,20–23} 1 in vitreous fluid,⁷ and 2 in plasma (ex vivo).^{16,24} The measurements were collected at field strengths ranging from 0.011 to 8.45 T and temperatures ranging from 21 to 40 $^{\circ}\text{C}$. 12 additional values of r_{1Ox} , measured in blood (ex vivo^{16,24,28} and in vivo^{20,29}) and tissues (lung³⁰ and brain³¹), were also found

(provided in Supplementary Table S2); however, these were not included in the model fitting because blood and tissues will contain factors not accounted for in this model (see Section 4).

The final values for the four parameters C_1 , C_2 , C_3 , and C_{Temp} (with lower and upper 95% confidence intervals) are listed in Table 2. The predicted versus true $r_{1\text{Ox}}$ values are plotted against the line of equality (solid black line) and a linear regression (dotted line, $R^2 = 0.93$) in Figure 3A, with a final mean squared error (MSE) of $0.19 \times 10^{-4} \text{ (s}^{-1}/\text{mmHg)}^2$. To examine bias in the model with respect to $r_{1\text{Ox}}$, B_0 , and temperature variables, Bland-Altman plots are provided in Figure 3B-D. The performance of the model on the subsets of water measurements only ($R^2 = 0.94$) and saline measurements only ($R^2 = 0.73$) is provided in Supplementary Figure S3.

The modelled versus measured $r_{1\text{Ox}}$ values from the randomized unseen test set of each iteration is plotted in Supplementary Figure S2A alongside the line of equality and the linear regression ($R^2 = 0.90$, $\text{MSE} = 0.26 \times 10^{-4} \text{ s}^{-1}/\text{mmHg}^2$). The difference between the modelled and measured $r_{1\text{Ox}}$ values from the randomized unseen test set of each iteration is illustrated as Bland-Altman plots in Supplementary Figure S2B-D.

To understand the behavior of the resulting model, the effect of varying field strength on $r_{1\text{Ox}}$ is illustrated using synthetic data under varying temperatures (Figure 4), and the linear effect of varying temperature on $r_{1\text{Ox}}$ is illustrated using synthetic data under varying field strengths (Supplementary Figure S4). The resulting model prediction is also shown over a scatterplot of the $r_{1\text{Ox}}$ of the 28 literature points in Figure 5.

Since Equation 5 contains four parameters, the fitting process was repeated for all combinations of fewer parameters (eg removing C_{Temp}) and the Akaike information criterion (AIC) was calculated for each version of the model—the best-fit model according to the AIC is the model that explains the greatest amount of variation using the fewest possible independent variables.³² The AIC score, R^2 , and MSE results of the different models tested are listed in Supplementary Table S3. The model with all four parameters scored the highest according to the AIC, and was therefore used in this manuscript. Removing only C_3 produced the second-highest AIC score, and removing only C_{Temp} produced the third-highest AIC score. The resulting predicted versus true $r_{1\text{Ox}}$ values and parameter distributions from each model are shown in Supplementary Figure S5.

4 | DISCUSSION

We have compiled empirical measurements of the relaxivity of oxygen over 50 years of MRI research in phantoms, saline and water solutions, plasma, and vitreous fluid, ranging from 0.011 to 8.45 T and 21 to 40 °C. While the reported relaxivity of oxygen varied greatly, we found that in the solutions of water, saline, vitreous fluid, and plasma the variance could largely be explained by the differences in field strength and

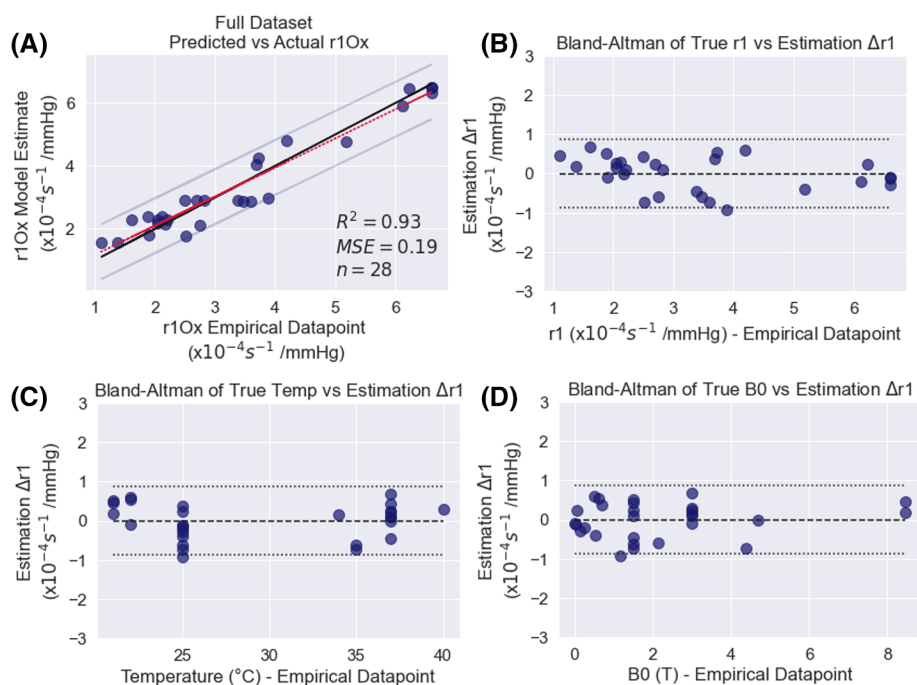


FIGURE 3 A, The modelled versus measured $r_{1\text{Ox}}$ values, plotted against the line of equality (solid black line) and a linear regression (red dotted line, $R^2 = 0.93$). B, A Bland-Altman plot showing the difference between the modelled and measured values of $r_{1\text{Ox}}$. C, D, Bland-Altman plots for the error in modelled $r_{1\text{Ox}}$ against temperature (C) and field strength (D) are also shown to examine bias in the model. The horizontal long-dashed lines show the mean value of $\Delta r_{1\text{Ox}}$ ($-0.005 \text{ s}^{-1} \times 10^{-4}/\text{mmHg}$), and the horizontal dotted lines show the limits of agreement (long dashes, calculated from $\text{mean}(\Delta r_{1\text{Ox}}) \pm 1.96 \text{ SD}(\Delta r_{1\text{Ox}})$)

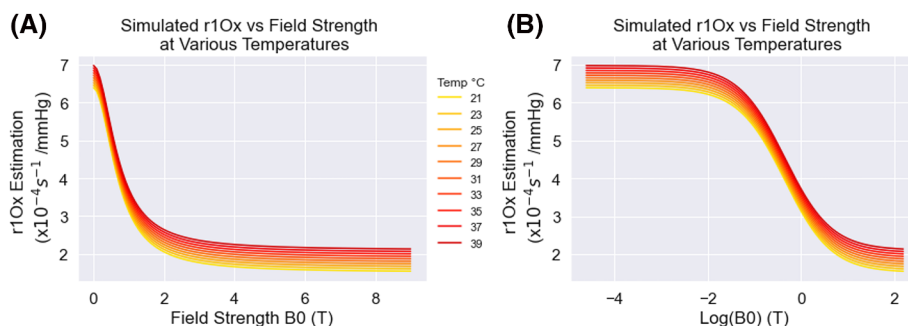


FIGURE 4 Plots with simulated data to illustrate the behavior of Equation 5 (with the fit parameter values) with respect to B_0 (A) and $\log(B_0)$ (B) for a variety of temperatures

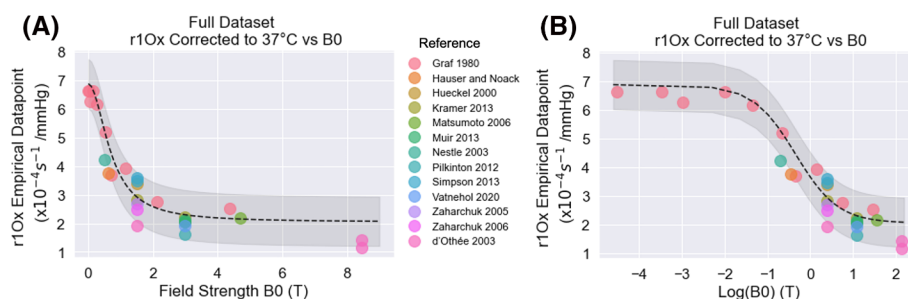


FIGURE 5 The r_{1Ox} of the 28 literature points, plotted against field strength (A) and $\log(\text{field strength})$ (B) alongside the r_{1Ox} estimated using the new model (black dashed line) at the appropriate B_0 and 37 °C, with the 95% confidence interval shown in grey. For this plot only, each literature value has been linearly corrected to 37 °C using the C_{Temp} parameter

temperature, and that this variation was well approximated by a Lorentzian function and linear relationship with temperature. Therefore, while the table of reported r_{1Ox} empirical measurements can be referred to for future oxygen-MRI experiments, the r_{1Ox} can also be estimated using the proposed simplified model for estimating the r_{1Ox} in water, saline, plasma, and vitreous fluids that agrees well with the empirical measurements.

The relationship between longitudinal relaxation and the paramagnetism of oxygen has a long history in NMR, and there is a large body of both theoretical and empirical work.^{1,14,15,33–37} For materials containing paramagnetic contrast agents, there can be complex relationships between R_1 and field strength, and these relationships are affected by various factors inherent to the contrast agent.³⁸ This relationship between contrast agent relaxivity and the magnetic field is important, as it can obscure the reproducibility of MRI-oxygen experiments if performed at different field strengths and temperatures.

The physical mechanisms that explain the relationship between field strength and relaxivity are complex, and although there are sophisticated explanations for specific contrast agents,^{39–42} much of the modelling of this relaxivity relies on empirical measurements.⁴³ While there has been previous evidence for modelling relaxivity- B_0 relationships as linear⁴⁴ or logarithmic,⁴⁵ one major limitation is that the majority of relaxivity measurements of contrast agents are performed at only two field strengths (1.5 and 3 T), which makes it difficult to properly describe the true relationship from empirical results. Interestingly, to address this issue, an experiment by Chou et al measured the relaxivity of a gadolinium-based contrast agent at a large range of field strengths, 0–12 T, revealing a curve that peaks around 1–2 T and drops off (in a Lorentzian shape) as field strength increases.³⁹ While these data are from a gadolinium-based contrast agent rather than oxygen, they suggest that the relationship of oxygen relaxivity and magnetic field strength may also follow a more complex curve than simply linear, or logarithmic. Therefore, for any modelling of relaxivity, it is important to state the range of field strengths over which the model is valid. The lowest field strength used to fit this model was 0.011 T, and below this field strength it is likely that the r_{1Ox} curves back down to zero as field strength approaches zero, in a similar manner to the pattern seen in Figure 4 of Chou et al,³⁹ which we have reproduced in Supplementary Figure S6.

4.1 | Limitations

The relaxivity values collected were from experiments performed over a timespan of five decades, with a huge variation in experimental equipment and temperature measurement techniques. Experimental measurement of r_{1Ox} can be difficult even within a relatively simple system

such as water, because the measurement accuracy depends on the proper selection of acquisition protocols and parameters (ie repetition and inversion times). For convenience, acquisition details from each experiment used in developing the present model are listed in Supplementary Table S4. MRI technology has advanced significantly since the measurements made in the 1980s, which account for the measurements made below 0.5 T, and low-field systems usually also suffer from poor signal to noise ratio. In addition, the values have often been extracted from original plots, some hand drawn, which is a source of error, and converted from the various original units to s^{-1}/mmHg , which can be another source of error. Finally, one experiment did not report the temperature of the solution during the experiment, and it was assumed to be 37 °C. These limitations inevitably represent a large source of potential error in the accuracy of this model. It is hoped, however, that this can be addressed as the NMR community produces new measurements of $r_{1\text{Ox}}$ at a range of field strengths and temperatures. As a future direction of this work, we have hosted the open-source model code and current $r_{1\text{Ox}}$ measurements on GitHub (github.com/BulteGroup/OxygenRelaxivityModel) and invite the NMR community to share new $r_{1\text{Ox}}$ measurement results and refit the model to improve the accuracy and enhance the utility of the model.

Furthermore, for the fitting of this model, we have combined values from water, saline, plasma, and vitreous fluids. In reality, there are factors that would cause the relaxivity in these solutions to differ, even amongst saline solutions with different compositions and concentrations. The decision to combine them was due to a lack of sufficient data points at a range of field strengths and temperatures in each solution; however, this is a considerable limitation, as it seems to fit more accurately to the water samples ($R^2 = 0.94$) than saline samples ($R^2 = 0.73$) alone (Supplementary Figure S3). Most importantly, values from the vitreous fluid and plasma would ideally be fit with separate models, as there are extra proteins in the plasma and vitreous fluid that have been shown to decrease the relaxivity slightly.^{7,16} However, this simply was not possible due to a lack of available data points in the literature. As above, we very much hope that this issue will be addressed as new data are acquired by future researchers.

Finally, this model does not represent the $r_{1\text{Ox}}$ in blood and tissues, where the addition of proteins, lipids, and deoxyhemoglobin will affect the R_1 - $p\text{O}_2$ relationship; however, we have created a separate general model to calculate the R_1 of blood, accounting for hematocrit, oxygen saturation, oxygen partial pressure, and magnetic field strength under hyperoxic conditions.⁴⁶ For convenience, however, we have listed the reported literature values found in tissue and blood in Supplementary Table S4—nine values from blood and three from tissues. For the purpose of this model, only the 28 $r_{1\text{Ox}}$ values in water, saline, vitreous fluid, and plasma were used.

5 | CONCLUSION

In conclusion, we have provided an overview of the literature reporting a relationship between longitudinal relaxation and oxygen in phantoms, saline and water solutions, and vitreous fluid ranging from 0.011 to 8.45 T and 21 to 40 °C. In addition, we have provided a simplified model for estimating the $r_{1\text{Ox}}$ in water, saline, plasma, and vitreous fluids that agrees well ($R^2 = 0.93$) with the empirical measurements. We hope that this will provide a useful resource for researchers seeking to quantify $p\text{O}_2$ in simple fluids, such as water and saline phantoms, or bodily fluids such as vitreous fluids, cerebrospinal fluids, and amniotic fluids.

ACKNOWLEDGEMENTS

EB is supported by funding from the Engineering and Physical Sciences Research Council (EPSRC) and Medical Research Council (MRC) (grant number EP/L016052/1) and the Clarendon Scholarship fund. DB and ES also gratefully acknowledge funding from the EPSRC (grant numbers EP/S021507/1 and EP/L024012/1).

DATA AVAILABILITY STATEMENT

Data sharing not applicable to this article as no datasets were generated or analysed during the current study.

ORCID

Emma Bluemke  <https://orcid.org/0000-0001-5970-9100>

Eleanor Stride  <https://orcid.org/0000-0003-3371-5929>

REFERENCES

- Mel'nichenko NA. The solubility of oxygen in sea water and solutions of electrolytes according to the pulse proton NMR data. *Russ J Phys Chem A*. 2008;82(9):1533-1539. <https://doi.org/10.1134/S0036024408090239>
- Muir ER, Cardenas DP, Duong TQ. MRI of brain tissue oxygen tension under hyperbaric conditions. *NeuroImage*. 2016;133:498-503. <https://doi.org/10.1016/j.neuroimage.2016.03.040>
- Nestle N, Baumann T, Niessner R. Oxygen determination in oxygen-supersaturated drinking waters by NMR relaxometry. *Water Res*. 2003;37(14):3361-3366. [https://doi.org/10.1016/S0043-1354\(03\)00211-2](https://doi.org/10.1016/S0043-1354(03)00211-2)



4. Vatnehol SAS, Hol PK, Bjørnerud A, Amiry-Moghaddam M, Haglerød C, Storås TH. Effect of drinking oxygenated water assessed by in vivo MRI relaxometry. *J Magn Reson Imaging*. 2020;52(3):720-728. <https://doi.org/10.1002/jmri.27104>
5. Wang ZJ, Joe BN, Coakley FV, Zaharchuk G, Busse R, Yeh BM. Urinary oxygen tension measurement in humans using magnetic resonance imaging. *Acad Radiol*. 2008;15(11):1467-1473. <https://doi.org/10.1016/j.acra.2008.04.013>
6. Berkowitz BA, Wilson CA. Quantitative mapping of ocular oxygenation using magnetic resonance imaging. *Magn Reson Med*. 1995;33(4):579-581. <https://doi.org/10.1002/mrm.1910330419>
7. Simpson ARH, Dowell NG, Jackson TL, Tofts PS, Hughes EH. Measuring the effect of pars plana vitrectomy on vitreous oxygenation using magnetic resonance imaging. *Invest Ophthalmol Vis Sci*. 2013;54(3):2028-2034. <https://doi.org/10.1167/iovs.12-11258>
8. Muir ER, Zhang Y, Nateras OSE, Peng Q, Duong TQ. Human vitreous: MR imaging of oxygen partial pressure. *Radiology*. 2013;266(3):905-911. <https://doi.org/10.1148/radiol.12120777>
9. Zaharchuk G, Busse RF, Rosenthal G, Manley GT, Glenn OA, Dillon WP. Noninvasive oxygen partial pressure measurement of human body fluids in vivo using magnetic resonance imaging. *Acad Radiol*. 2006;13(8):1016-1024. <https://doi.org/10.1016/j.acra.2006.04.016>
10. Zaharchuk G, Martin AJ, Rosenthal G, Manley GT, Dillon WP. Measurement of cerebrospinal fluid oxygen partial pressure in humans using MRI. *Magn Reson Med*. 2005;54(1):113-121. <https://doi.org/10.1002/mrm.20546>
11. Dewhurst MW, Birer SR. Oxygen-enhanced MRI is a major advance in tumor hypoxia imaging. *Cancer Res*. 2016;76(4):769-772. <https://doi.org/10.1158/0008-5472.can-15-2818>
12. Little RA, Jamin Y, Boulton JKR, et al. Mapping hypoxia in renal carcinoma with oxygen-enhanced MRI: comparison with intrinsic susceptibility MRI and pathology. *Radiology*. 2018;288(3):739-747. <https://doi.org/10.1148/radiol.2018171531>
13. O'Connor JPB, Robinson SP, Waterton JC. Imaging tumour hypoxia with oxygen-enhanced MRI and BOLD MRI. *Br J Radiol*. 2019;92(1095):20180642. <https://doi.org/10.1259/bjr.20180642>
14. Chiarotti G, Cristiani G, Giulotto L. Proton relaxation in pure liquids and in liquids containing paramagnetic gases in solution. *Nuovo Cimento*. 1955;1(5):863-873. <https://doi.org/10.1007/bf02731333>
15. Bloembergen N. Proton relaxation times in paramagnetic solutions. *J Chem Phys*. 1957;27(2):572-573. <https://doi.org/10.1063/1.1743771>
16. d'Othée BJ, Rachmuth G, Munasinghe J, Lang EV. The effect of hyperoxygenation on T1 relaxation time in vitro. *Acad Radiol*. 2003;10(8):854-860. [https://doi.org/10.1016/s1076-6332\(03\)00004-7](https://doi.org/10.1016/s1076-6332(03)00004-7)
17. Teng CL, Hong H, Kihne S, Bryant RG. Molecular oxygen spin-lattice relaxation in solutions measured by proton magnetic relaxation dispersion. *J Magn Reson*. 2001;148(1):31-34. <https://doi.org/10.1006/jmre.2000.2219>
18. Matsumoto K, Bernardo M, Subramanian S, et al. MR assessment of changes of tumor in response to hyperbaric oxygen treatment. *Magn Reson Med*. 2006;56(2):240-246. <https://doi.org/10.1002/mrm.20961>
19. Kramer H, Corcos A, Hernando D, Berry J, Schiebler M, Reeder S. Effekt von molekularem Sauerstoff auf Relaxationszeiten bei klinischen Feldstärken. *Fortschr Röntgenstr*. 2013;103(S 01):185. <https://doi.org/10.1055/s-0033-1346217>
20. Pilkinton DT, Hiraki T, Detre JA, Greenberg JH, Reddy R. Absolute cerebral blood flow quantification with pulsed arterial spin labeling during hypoxia corrected with the simultaneous measurement of the longitudinal relaxation time of arterial blood. *Magn Reson Med*. 2012;67(6):1556-1565. <https://doi.org/10.1002/mrm.23137>
21. Vatnehol SAS, Hol PK, Bjørnerud A, Amiry-Moghaddam M, Haglerød C, Storås TH. Determination of oxygen r_1 at 3 Tesla using samples with a concentration range of dissolved oxygen. *Magn Reson Mater Phys Biol Med*. 2020;33(3):447-453. <https://doi.org/10.1007/s10334-019-00783-x>
22. Hausser R, Noack F. Kernmagnetische Relaxation und Korrelation im System Wasser-Sauerstoff. *Z Naturforsch A*. 1965;20(12):1668-1675. <https://doi.org/10.1515/zna-1965-1220>
23. Graf V, Noack F, Béné GJ. Proton spin T_1 relaxation dispersion in liquid H₂O by slow proton-exchange. *J Chem Phys*. 1980;72(2):861-863. <https://doi.org/10.1063/1.439240>
24. Hueckel P, Schreiber W, Markstaller K, Bellemann M, Kauczor H-U, Thelen M. Effect of partial oxygen pressure and hematocrit on T1 relaxation in human blood. *Proc Int Soc Magn Reson Med*. 2000;8:1586.
25. Rohatgi A. *WebPlotDigitizer*. <https://automeris.io/WebPlotDigitizer/citation.html>. Accessed June 29, 2021.
26. Virtanen P, Gommers R, Oliphant TE, et al. SciPy 1.0: fundamental algorithms for scientific computing in Python. *Nat Methods*. 2020;17(3):261-272. <https://doi.org/10.1038/s41592-019-0686-2>
27. Pedregosa F, Varoquaux G, Gramfort A, et al. Scikit-learn: machine learning in Python. *J Machine Learn Res*. 2011;12(85):2825-2830.
28. Silvennoinen MJ, Kettunen MI, Kauppinen RA. Effects of hematocrit and oxygen saturation level on blood spin-lattice relaxation. *Magn Reson Med*. 2003;49(3):568-571. <https://doi.org/10.1002/mrm.10370>
29. Tripathi A, Bydder GM, Hughes JMB, et al. Effect of oxygen tension on NMR spin-lattice relaxation rate of blood in vivo. *Invest Radiol*. 1984;19(3):174-178. <https://doi.org/10.1097/00004424-198405000-00004>
30. Campbell-Washburn AE, Ramasawmy R, Restivo MC, et al. Opportunities in interventional and diagnostic imaging by using high-performance low-field-strength MRI. *Radiology*. 2019;293(2):384-393. <https://doi.org/10.1148/radiol.2019190452>
31. Beeman SC, Shui Y-BB, Perez-Torres CJ, Engelbach JA, Ackerman JJ, Garbow JR. O₂-sensitive MRI distinguishes brain tumor versus radiation necrosis in murine models. *Magn Reson Med*. 2016;75(6):2442-2447. <https://doi.org/10.1002/mrm.25821>
32. Bozdogan H. Model selection and Akaike's information criterion (AIC): the general theory and its analytical extensions. *Psychometrika*. 1987;52(3):345-370. <https://doi.org/10.1007/BF02294361>
33. Parker DS, Harmon JF. Dipolar spin-lattice relaxation in water containing oxygen. *Chem Phys Lett*. 1974;25(4):505-506. [https://doi.org/10.1016/0009-2614\(74\)85353-4](https://doi.org/10.1016/0009-2614(74)85353-4)
34. Mirhej ME. Proton spin relaxation by paramagnetic molecular oxygen. *Can J Chem*. 1965;43(5):1130-1138. <https://doi.org/10.1139/v65-150>
35. Solomon I. Relaxation processes in a system of two spins. *Phys Rev*. 1955;99(2):559-565. <https://doi.org/10.1103/PhysRev.99.559>
36. Torrey HC. Nuclear spin relaxation by translational diffusion. *Phys Rev*. 1953;92(4):962-969. <https://doi.org/10.1103/PhysRev.92.962>
37. Young IR, Clarke GJ, Baffles DR, Pennock JM, Doyle FH, Bydder GM. Enhancement of relaxation rate with paramagnetic contrast agents in NMR imaging. *J Comput Tomogr*. 1981;5(6):543-547. [https://doi.org/10.1016/0149-936X\(81\)90089-8](https://doi.org/10.1016/0149-936X(81)90089-8)
38. Rohrer M, Bauer H, Mintorovitch J, Requardt M, Weinmann H-J. Comparison of magnetic properties of MRI contrast media solutions at different magnetic field strengths. *Invest Radiol*. 2005;40(11):715-724. <https://doi.org/10.1097/01.rli.0000184756.66360.d3>

39. Chou C-Y, Abdesslem M, Bouzigues C, et al. Ultra-wide range field-dependent measurements of the relaxivity of $Gd_{1-x}Eu_xVO_4$ nanoparticle contrast agents using a mechanical sample-shuttling relaxometer. *Sci Rep*. 2017;7(1):44770. <https://doi.org/10.1038/srep44770>
40. Fischer HW, Rinck PA, van Haverbeke Y, Muller RN. Nuclear relaxation of human brain gray and white matter: analysis of field dependence and implications for MRI. *Magn Reson Med*. 1990;16(2):317-334. <https://doi.org/10.1002/mrm.1910160212>
41. Kirsch JE. Basic principles of magnetic resonance contrast agents. *Top Magn Reson Imaging*. 1991;3(2):1-18.
42. Koenig SH, Baglin C, Brown RD, Brewer CF. Magnetic field dependence of solvent proton relaxation induced by Gd^{3+} and Mn^{2+} complexes. *Magn Reson Med*. 1984;1(4):496-501. <https://doi.org/10.1002/mrm.1910010408>
43. Elster AD. How much contrast is enough? Dependence of enhancement on field strength and MR pulse sequence. *Eur Radiol*. 1997;7(Suppl 5):276-280. <https://doi.org/10.1007/pl00006908>
44. Hales PW, Kirkham FJ, Clark CA. A general model to calculate the spin-lattice (T_1) relaxation time of blood, accounting for haematocrit, oxygen saturation and magnetic field strength. *J Cereb Blood Flow Metab*. 2016;36(2):370-374. <https://doi.org/10.1177/0271678X15605856>
45. Wang Y, van Gelderen P, de Zwart JA, Duyn JH. B_0 -field dependence of MRI T_1 relaxation in human brain. *NeuroImage*. 2020;213:116700. <https://doi.org/10.1016/j.neuroimage.2020.116700>
46. Bluemke E, Stride E, Bulte DP. A general model to calculate the spin-lattice relaxation rate (R_1) of blood, accounting for haematocrit, oxygen saturation, oxygen partial pressure, and magnetic field strength under hyperoxic conditions. *J Magn Reson Imaging*. <https://doi.org/10.1002/jmri.27938>, In press.

SUPPORTING INFORMATION

Additional supporting information may be found in the online version of the article at the publisher's website.

How to cite this article: Bluemke E, Stride E, Bulte DP. A simplified empirical model to estimate oxygen relaxivity at different magnetic fields. *NMR in Biomedicine*. 2022;35(2):e4625. doi:10.1002/nbm.4625

